Solar Energy Materials & Solar Cells 157 (2016) 510–516

Contents lists available at ScienceDirect

Solar Energy Materials & Solar Cells

journal homepage: www.elsevier.com/locate/solmat

Hexadecafluorophthalocyaninatocopper as an electron conductor for high-efficiency fullerene-free planar perovskite solar cells

Fangming Jin [a], Chengyuan Liu [a,b], Fuhua Hou [a,b], Qiaogang Song [a,b], Zisheng Su [a,*], Bei Chu [a], Pengfei Cheng [c], Haifeng Zhao [a], Wenlian Li [a]

[a] State Key Laboratory of Luminescence and applications, Changchun Institute of Optics, Fine Mechanics, and Physics, Chinese Academy of Sciences, Changchun130033, PR China
[b] University of Chinese Academy of Sciences, Beijing 100039, PR China
[c] School of Aerospace Science and Technology, Xidian University, Xi'an 710126, PR China

ARTICLE INFO

Article history:
Received 19 May 2016
Received in revised form
19 July 2016
Accepted 23 July 2016
Available online 27 July 2016

Keywords:
Perovskite solar cells
Electron transport layer
F_{16}CuPc
Fullerene-free
High-efficiency

ABSTRACT

High-efficiency fullerene-free planar perovskite solar cells (PSCs) consisting of hexadecafluorophthalocyaninatocopper (F_{16}CuPc) as electron conductors are firstly reported. In the condition of using F_{16}CuPc as a direct replacement for fullerene that universally employed in planar PSCs with an architecture of ITO/hole transport layer (HTL)/perovskite/electron transport layer (ETL), PSCs exhibit quite satisfactory photovoltaic performances. The best PSC with F_{16}CuPc ETL presents a power conversion efficiency of 12.62% with a short-circuit current density (J_{SC}) of 19.97 mA/cm^2, an open-circuit voltage (V_{OC}) of 0.93 V and a fill factor (FF) of 0.68. Such performance is comparable to the C_{60}-based PSCs and higher than that of the PCBM-based PSCs.

1. Introduction

Over the past few years, people have most recently witnessed a rapid development and a major breakthrough in perovskite solar cells (PSCs) based on organic metal halide as light harvesters [1–5]. Due to their remarkable power conversion efficiency (PCE) along with very low material costs, organic metal halide PSCs have been regarded as promising technology for solar energy conversion to tackle the energy and environment problems that threaten sustainable development of human society. To date, two typical structures, i.e., a mesoscopic nanostructure and a planar structure can be constructed to form an efficient PSC [6]. The planar PSC possesses a much simpler structure and a substantial lower manufacturing temperature and might be more promising compared with the mesoscopic nanostructure device. To realize high-efficiency PSCs, electron transport layer (ETL) is more important than hole transport layer (HTL), which lies in the fact that holes can be extracted more efficiently than electrons in perovskite [7,8]. A variety of organic or inorganic electron conductor materials, including C_{60}, PCBM, TiO_2, Al_2O_3, ZnO and etc. have been successfully applied in PSCs [8–11]. Although inorganic electron conductors present higher stability and better electron mobility compared with their organic counterparts, they require upper dependability on temperature and equipments to realize ETL with high quality. As a result, fullerene-based materials such as C_{60} and PCBM are commonly used as the electron conductor component in planar architecture PSCs of ITO/HTL/perovskite/ETL [12–15]. In the field of organic solar cell (OSC) research, development of non-fullerene acceptors remains an issue as weak absorption in the visible region and relative low LUMO energy level of fullerene [16,17]. This may not hold completely true for PSCs while, unfortunately, fullerene is very unstable in light and ambient air environment [18–20]. Thus, fullerene is not a perfect ETL material from consideration of device stability, and it is also desirable to develop new electron conductor to replace the use of fullerene in PSCs. Besides, development of new charge conduct materials is particularly meaningful in providing optional opportunity to match different energy band levels of various perovskite materials no matter in the field of perovskite photovoltaics or in perovskite light-emitting diodes (PerLEDs).

Metallophthalocyanines (MPcs) which have been widely used as electron donor material in OSCs, show reasonable ambipolar carrier transporting properties for efficient charge transfer [21]. A copper phthalocyanine (CuPc) derivative of hexadecafluorophthalocyaninatocopper (F_{16}CuPc) was successfully applied as n-channel semiconducting material to construct air-stable organic thin-film transistors (OTFTs) [22]. In the present study, we demonstrate the fabrication of planar PSCs comprised of

* Corresponding author.
E-mail address: suzs@ciomp.ac.cn (Z. Su).

http://dx.doi.org/10.1016/j.solmat.2016.07.037
0927-0248/

$CH_3NH_3PbI_3$ as light harvester and $F_{16}CuPc$ as electron conductor for the first time. An outstanding short-circuit current density of 19.97 mA/cm^2 and power conversion efficiency (PCE) of 12.62% were achieved for the $CH_3NH_3PbI_3$ devices with $F_{16}CuPc$ as ETL, which is comparable to the device employing a fullerene electron conductor.

2. Experimental section

2.1. Materials and device fabrication

Materials were all obtained from commercial resources and used as received without any further purification. Device Structural illustration is displayed in Fig. 1. Solar cells with the configuration of ITO/PEDOT: PSS (40 nm)/$CH_3NH_3PbI_3$ (~350 nm)/$F_{16}CuPc$/BPhen (10 nm)/Al (100 nm) were fabricated on precleaned indium tin oxide (ITO)-coated glass substrates with a sheet resistance of 15 Ωsq^{-1}. The ITO surface was cleaned in a series of solvents of acetone, deionized water and acetone, and then treated by ultraviolet-ozone in a chamber for 10 min. PEDOT: PSS was spin-coated on an ITO surface under 3500 rpm for 40 s to form the thickness of about 40 nm and then annealed at 120 °C for 15 min on hot plate.

The $CH_3NH_3PbI_3$ absorber layer was deposited by the two-step deposition method [10,11,23,24]. First, 460 mg/ml PbI_2 dissolved in N,N-dimethylformamide (DMF) was spin-coated onto the PEDOT: PSS film at a speed of 3000 rpm for 30 s and then heat treated at 100 °C for a while to remove the DMF solvent. Immediately, 50 mg/ml CH_3NH_3I dissolved in propanol was spin-coated onto the PbI_2 film at a speed of 3000 rpm for 30 s. After this spinning procedure, the $CH_3NH_3PbI_3$ absorber layer obtained were then heated at 100 °C for 60 min in air on a hot plate to finish the formation of $CH_3NH_3PbI_3$ perovskite film. After cooling to room temperature, perovskite film was transferred into the high vacuum system (5×10^{-4} Pa) to deposit organic layers and mental electrode. $F_{16}CuPc$, BPhen (10 nm) and Al (100 nm) were sequentially evaporated on the $CH_3NH_3PbI_3$ perovskite. The thickness was monitored by a quartz crystal monitor. To probe the effect of $F_{16}CuPc$ layer on device performances, devices were prepared by depositing different thickness of 0, 10, 20, 40 and 60 nm $F_{16}CuPc$. BPhen is widely used as exciton blocking layers (EBLs) in OSCs. In our PSCs here, we used BPhen as a cathode buffer layer to form an Ohmic contact between organic ETLs and Al electrode, similar with some previous results [25]. Finally, the device was completed by thermal evaporation of Al as a negative electrode through a shadow mask to define the active device area of 10 mm^2. PSCs with a thermal evaporated C_{60} and a spin-coated PCBM as ETLs were also fabricated as the reference devices.

2.2. Measurements

Current density -voltage (J-V) characteristics of the devices were measured with a Keithley 2400 source meter both in dark and illuminated with a Xe lamp with an AM 1.5 G filter, and the irradiation intensity was certified to be 100 mW/cm^2. The voltage scans were swept from short circuit to forward bias with a rate of 0.02 Vs^{-1} unless otherwise specified. The incident photon to current conversion efficiency (IPCE) spectra were performed with a Stanford SR803 lock-in amplifier under monochromatic illumination at a chopping frequency of 110 Hz by a Stanford SR540 chopper. X-ray diffraction (XRD) patterns were recorded with a Rigaku D/Max-2500 diffractometer using Cu Kαradiation (λ=1.54 Å). Absorption spectra were recorded with a Shimadzu UV-3101PC spectrophotometer. For the film absorption spectra measurements, $CH_3NH_3PbI_3$ perovskite film was also fabricated on the ITO/PEDOT: PSS substrate and its parasite absorption were excluded by using ITO/PEDOT: PSS substrate as the reference sample in the experiments. Steady-state photoluminescent (PL) spectra were measured using a UV-lamp spectroscope FL-920 with a semiconductor laser at 492 nm. The surface topographies were imaged with a Bruker MultiMode 8 at. force microscope (AFM) in tapping mode. Scanning electron microscopy (SEM) images were measured on a Hitachi S4800. Device fabrication and the measurements were all carried out under ambient conditions with a humidity of about 20–30% at room temperature.

3. Results and discussions

The inset of Fig. 2 displays photographs of the patterned Glass /ITO/PEDOT: PSS/PbI_2 (top) and Glass/ITO/PEDOT:PSS/$CH_3NH_3PbI_3$ (bottom) substrate for comparison. Transformation from PbI_2 to $CH_3NH_3PbI_3$ resulted in a dramatically change in the color from yellow to black and brown. The transformation of crystalline structure on the glass/ITO/PEDOT:PSS substrate was characterized by XRD, and the results are included in Fig. 2. Four diffraction peaks of 12.7°, 25.5°, 38.7° and 52.3° corresponding to the lattice planes of (001), (002), (003) and (004) for PbI_2 were clearly detected in the Glass/ITO/PEDOT: PSS/PbI_2 sample. The diffraction peaks of 35.3° and 50.7° belong to ITO substrate corresponding to the signal of (400) and (440) [26]. In the Glass/ITO/PEDOT: PSS/$CH_3NH_3PbI_3$ sample, a series of strong peaks appeared at 14.1°, 28.5°, 31.9° and 43.3°, which are assigned to the (110), (220), (310) and (330) of $CH_3NH_3PbI_3$ crystal, indicating an orthorhombic crystal structure of halide perovskite with high crystallinity [27]. It is noted that if $CH_3NH_3PbI_3$ film has impurity of PbI_2, signature peak at 12.7° will be observed. In the present $CH_3NH_3PbI_3$ film here, the disappearance of the aforementioned peak suggests a

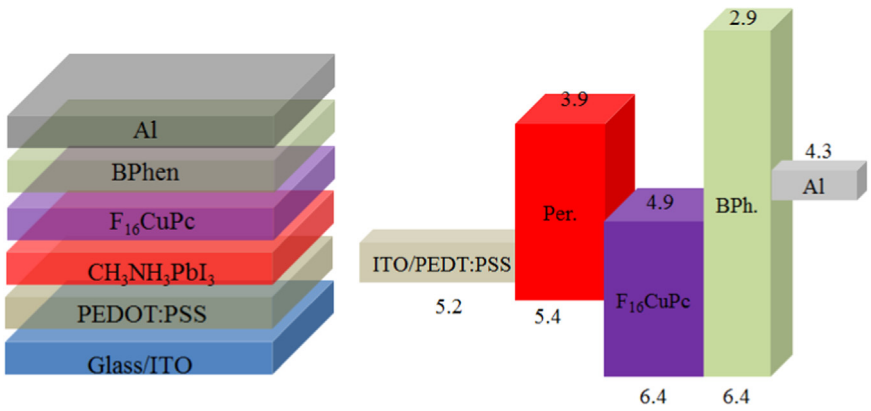

Fig. 1. (a) Structural illustration of device fabrication. (b) Schematic illustration of the energy diagram of the devices.

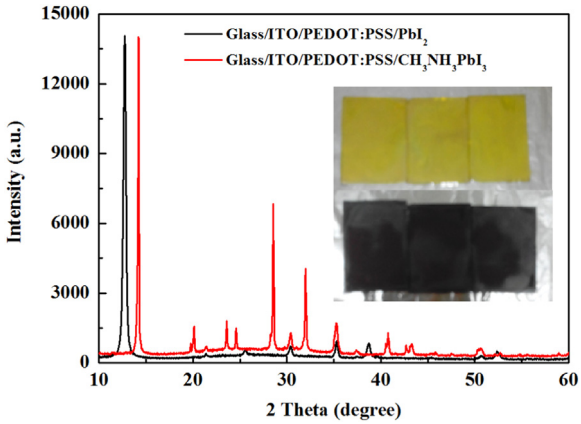

Fig. 2. GAXRD patterns of the Glass/ITO/PEDOT:PSS/PbI_2 and Glass/ITO/PEDOT:PSS/$CH_3NH_3PbI_3$. Inset: Photographs of the patterned Glass/ITO/PEDOT:PSS/PbI_2 and Glass/ITO/PEDOT:PSS/$CH_3NH_3PbI_3$.

complete consumption of PbI_2 via two-step deposition method here.

The morphology of $CH_3NH_3PbI_3$ perovskite film was characterized using scanning electron microscopy (SEM) and atomic force microscopy (AFM), with results presented in Fig. 3. Large $CH_3NH_3PbI_3$ crystallites with size of several hundred nanometers were observed. The large crystallites increase the carrier mobility and exciton diffusion length of the $CH_3NH_3PbI_3$ perovskite and reduce the recombination possibility from defect and trap states, which is beneficial to realize a high-performance device [28]. Typical cross-sectional SEM image shown in Fig. 3b indicates that the resulting perovskite film has a thickness of ~350 nm. The surface roughness of the film was measured by AFM (Fig. 3c, and d), and calculated to be 35 nm in the range of 3 μm × 3 μm which is in accordance with previous reports [29].

Typical absorption spectra of $CH_3NH_3PbI_3$, $F_{16}CuPc$ and $CH_3NH_3PbI_3/F_{16}CuPc$ film are presented in Fig. 4, along with the molecular structures of $F_{16}CuPc$ given in the inset. $CH_3NH_3PbI_3$ film absorbs a wide range of light from visible to the near-infrared, indicating the formation of $CH_3NH_3PbI_3$ perovskite on ITO/PEDOT:PSS substrate. The absorption of $CH_3NH_3PbI_3$ is extremely strong even that in the range of 310–470 nm, absorbance is beyond the detection limits of our equipment. $F_{16}CuPc$ absorbs light across broad wavelength ranging from 300 to 450 nm and from 550 to 800 nm. Although light extinction of $F_{16}CuPc$ is nearly over the whole visible range, the absorption intensity is much weaker and is negligible compared with the perovskite layer considering the excellent light absorbility of $CH_3NH_3PbI_3$. This was confirmed by the little difference of absorption spectra observed between $CH_3NH_3PbI_3$ and $CH_3NH_3PbI_3$/40 nm $F_{16}CuPc$ films. As a result, it is unnecessary to take the absorption influence of $F_{16}CuPc$ into account when constructs a PSC device no matter excitons generated in $F_{16}CuPc$ can be dissociated at the interface of $CH_3NH_3PbI_3/F_{16}CuPc$ or not.

To determine the feasibility of $F_{16}CuPc$ as electron conductor in planar heterojunction configuration PSCs, we compared $CH_3NH_3PbI_3$ devices by varying the thickness of $F_{16}CuPc$ layer. The current-voltage (J-V) curves of the perovskite devices with various

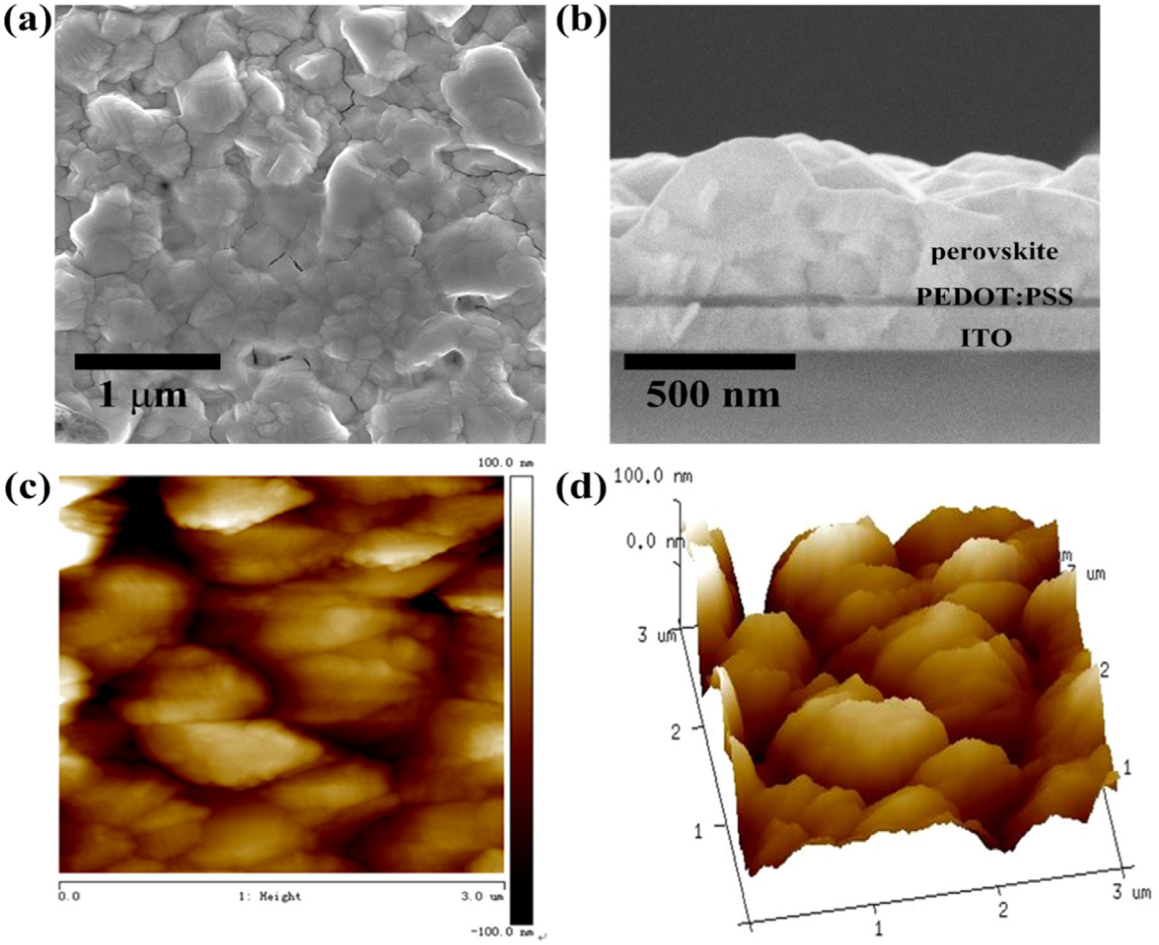

Fig. 3. The perovskite film grown on the ITO/PEDOT:PSS substrate by the two-step spin-coating procedure◆(a) Top-view SEM image ; (b) Cross-sectional SEM image; (c) 2D AFM height image; (d) 3D AFM height image.

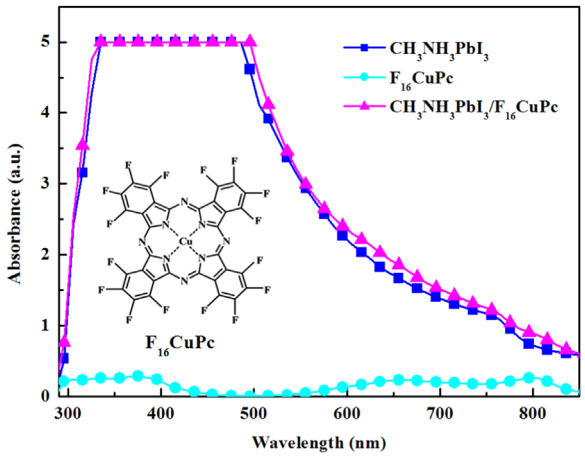

Fig. 4. Absorption spectra of $CH_3NH_3PbI_3$, 40 nm $F_{16}CuPc$ and $CH_3NH_3PbI_3$/40 nm $F_{16}CuPc$. The inset shows the molecular structure of $F_{16}CuPc$.

thickness of $F_{16}CuPc$ as ETL are shown in Fig. 5a, and corresponding photovoltaic parameters are summarized in Table 1. The statistical performances were extracted over 24 samples for each device. Performance of the devices is strictly dependent upon the thickness of $F_{16}CuPc$ and the best cell is obtained at a $F_{16}CuPc$ thickness of 40 nm. Device without $F_{16}CuPc$ delivered a short-circuit current density (Jsc) of 6.85 mA/cm^2, an open-circuit voltage (Voc) of 0.34 V and a fill factor (FF) of 0.30, leading to a PCE of 0.71% under standard AM1.5 G illumination. Interestingly, planar devices without an electron conductor or acceptor deliver a photocurrent beyond 6 mA/cm^2. Two reasons may account for this. One is that perovskite functions as the absorber and the electron transporter simultaneously, and exciton dissociation occurs efficiently in the bulk. The other is that interface between PEDOT: PSS and $CH_3NH_3PbI_3$ could potentially act as hybrid Schottky heterojunction for exciton dissociation due to the existence of an internal electric field across the interface. Despite of impressive photocurrent obtained, the FF and Voc are very low for the devices without ETL because of the increased recombination at cathode side and a corresponding low shunt resistance. Due to the good hole transporting property of perovskite $CH_3NH_3PbI_3$, the photogenerated electrons and holes can recombine strongly at the interface of perovskite layer and negative electrode [2,30]. Incorporating even a thin 10 nm $F_{16}CuPc$ layer into the device suppresses the recombination and substantially improves both the Voc and the FF. For the device with 40 nm $F_{16}CuPc$, PCEs in excess of 11% were realized and the best cell offered a PCE 12.52% with a

Table 1
Performance summary of the devices with various thickness of $F_{16}CuPc$ as ETL.

Thickness of $F_{16}CuPc$	Jsc (mA/cm^2)	Voc (V)	FF	PCE (%)
0	6.85 ± 1.76	0.34 ± 0.02	0.30 ± 0.07	0.71 ± 0.33
10	13.51 ± 1.56	0.74 ± 0.03	0.39 ± 0.06	3.89 ± 0.82
20	16.21 ± 2.30	0.82 ± 0.03	0.51 ± 0.04	6.89 ± 1.59
40	18.02 ± 2.45	0.92 ± 0.02	0.66 ± 0.04	11.06 ± 1.94
40 (best)	19.97	0.93	0.68	12.62
60	18.15 ± 2.23	0.90 ± 0.03	0.58 ± 0.03	9.59 ± 1.75

J_{SC} 19.97 mA/cm^2, a Voc of 0.93 V and an FF of 0.68. From the AFM images presented in Fig. 3c and d, a rough-textured $CH_3NH_3PbI_3/F_{16}CuPc$ interface is highly expected when constructs a solar cell. The rough interface improves the charge transport by decreasing the electron transport distance, while provides a more easily formation of the direct contact for $CH_3NH_3PbI_3$ with Al electrode [31]. This explains the reason that why a thicker $F_{16}CuPc$ layer is benefit to device performance. In the thin $F_{16}CuPc$ case, it is highly possible for $CH_3NH_3PbI_3$ and Al electrode to contact directly with each other, causing serious exciton quenching and charge recombination resulting in a low Jsc, FF and V_{OC}, hence the PCE. The reduction of FF and PCE with thickness of $F_{16}CuPc$ increased to 60 nm can be easily understood. As the thickness of $F_{16}CuPc$ increased from 40 nm to 60 nm, series resistance of the cell was inevitably increased and electron collection became difficult, leading to a reduced FF and hence the PCE. So there exists a tradeoff between hole and exciton blocking and electron transfer and the optimal thickness of $F_{16}CuPc$ was found to be 40 nm.

The IPCE spectra are provided in Fig. 5b. Identical spectrum shape for the devices with different thickness of $F_{16}CuPc$ was observed, which demonstrates the inference mentioned above that $CH_3NH_3PbI_3$ perovskite acts as the light absorber and is the primary contributor to the photocurrent and absorption influence of $F_{16}CuPc$ is negligible. Device shows a spectral response across almost the entire spectrum (300–800 nm) with a peak IPCE at approximately 550 nm, in agreement with the previous report [29]. For the optimized device with 40 nm $F_{16}CuPc$, efficiency above 65% was obtained across wide spectral coverage of 380–760 nm highlights the excellent performance for the device. The improved response with increase the thickness of $F_{16}CuPc$ was observed and is coincident with the enhancement of the photocurrent. Integrating the overlap of the IPCE spectrum with the AM1.5G solar photon flux yields a current density within a minor error compared with the measured photocurrent density, which confirms that the spectrum mismatch between the simulated sunlight and the AM1.5G standard can be ignored.

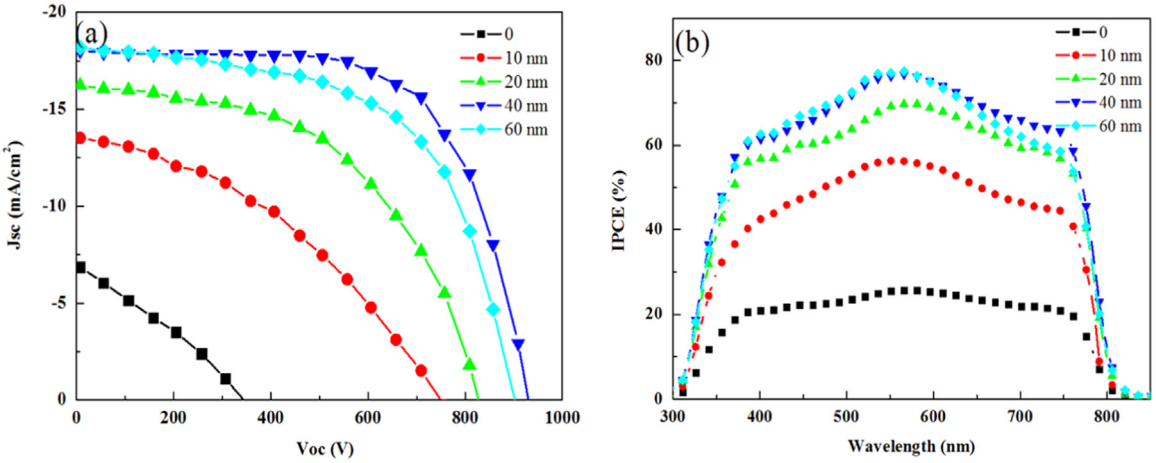

Fig. 5. (a) J–V curves and (b) IPCE spectra of the PSCs with various thickness of $F_{16}CuPc$ as ETL.

Table 2
Performance summary of the devices with different ETLs.

ETL	Jsc (mA/cm^2)	Voc (V)	FF	PCE (%)
F_{16}CuPc	18.02 ± 2.45	0.92 ± 0.02	0.66 ± 0.04	11.06 ± 1.94
PCBM	19.12 ± 2.27	0.91 ± 0.03	0.52 ± 0.06	9.04 ± 2.79
C_{60}	19.08 ± 2.30	0.94 ± 0.01	0.67 ± 0.04	12.01 ± 2.11

PSCs with spin-coated PCBM and thermal evaporated C_{60} as reference ETLs were also constructed to evaluate property of F_{16}CuPc as ETL in PSCs and their performance are summarized in Table 2 for comparison. It shows that devices with PCBM and C_{60} as ETLs deliver a PCE of 9.04% and 12.01% respectively, which is comparable to previous reports [12,15,28]. Our F_{16}CuPc-based devices show approximate photovoltaic performance with C_{60} devices while offer a 22% increase in PCE compared with the PCBM-based PSCs, which demonstrates bright prospect to use F_{16}CuPc as effective fullerene-free ETLs in PSCs. Besides, hysteresis of the planar PSC devices with different ETLs was studied and the typical hysteresis results are provided in Fig. 6. As we can see that little difference between the forward and reverse scanning is obtained for both F_{16}CuPc and C_{60} devices.

It is interesting to point out that for OSCs with F_{16}CuPc as electron acceptor, the reported efficiency is only 0.18% and 0.38% which is much smaller than C_{60}-based OSCs. While for the PSCs here, efficiencies obtained for F_{16}CuPc and C_{60} devices are comparable [32,33]. As displayed in the energy level diagram of the investigated cells in Fig. 1b, the LUMO and the HOMO levels of $CH_3NH_3PbI_3$ perovskite are –3.9 and −5.4 eV, and those of F_{16}CuPc are –4.9 and −6.2 eV, respectively. A donor–acceptor PHJ system can be successfully formed and electron transfer from $CH_3NH_3PbI_3$ perovskite to F_{16}CuPc is energetically favorable. The F_{16}CuPc ETL can block hole transport to the negative electrode effectively due to its deep HOMO level of 6.2 V. For organic small weight molecule and polymer solar cells based on donor-acceptor heterojunction, Voc approximately follows the empirical relationship of $Voc \approx (1/e)(|EHOMO\ donor| - |ELUMO\ acceptor|) - 0.3$, where e represents elementary charge, EHOMO donor represents the HOMO level of the donor, ELUMO acceptor represents the LUMO level of the acceptor and 0.3 is an empirical parameter related with the energy loss [34]. Applying such relationship to PSCs here, the calculated V_{OC} is only 0.2 V, a large disparity between our experiment results of over 0.9 V. Such disparity illustrates that photoinduced charge transfer processes in the PSCs here are entirely different from that in OSCs. If the interface of $CH_3NH_3PbI_3/F_{16}$CuPc is the only heterojunction that dissociates excitons, energy loss during charge

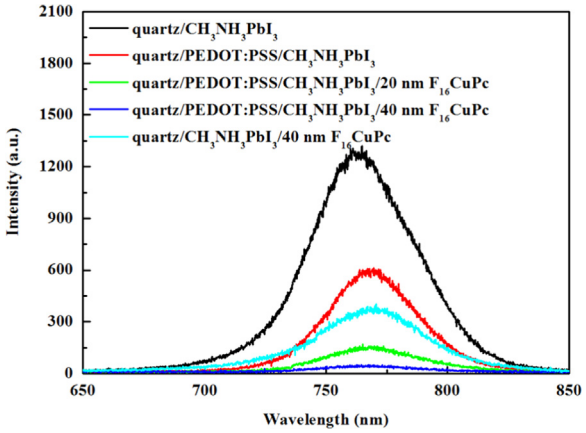

Fig. 7. Steady-state PL spectra for $CH_3NH_3PbI_3$ at an excited wavelength of 492 nm.

transfer between $CH_3NH_3PbI_3$ and F_{16}CuPc must cause a big Voc deficiency and a high Voc is hardly achieved. This is in accordance with the discussion above that devices without electron conductor F_{16}CuPc can deliver an impressive photocurrent and $CH_3NH_3PbI_3$ perovskite itself can function as hole and electron conductor, and excitons generated in $CH_3NH_3PbI_3$ can be separated in $CH_3NH_3PbI_3$ bulk. Actually, mechanism and dynamics of charge generation of planar perovskite solar cells have been studied and more and more results show that exciton binding energies in the room-temperature phase possibly as low as ~1–10 meV [35]. Free charges are expected to generated spontaneously following light absorption, as opposed to a large population of bound excitons [36]. Recent report showed that for $CH_3NH_3PbI_3$ perovskite, both excitons and free carriers are photogenerated at a short time with an estimated ratio of ~1:10, indicating that photocarriers dominate the photoexcitations in neat perovskites [37]. All these discussions explain the excellent performance of F_{16}CuPc-based PSCs and the big performance discrepancy of the OSCs and PSCs employing F_{16}CuPc as the electron acceptor or conductor layer.

To further evaluate the effect of the F_{16}CuPc layer in the PSCs, photoluminescence (PL) measurement which is a simple and valid way to investigate charge separation was applied, and the photoluminescence results are shown in Fig. 7. When $CH_3NH_3PbI_3$ was deposited onto quartz substrate, strong photoluminescence from $CH_3NH_3PbI_3$ was observed centered at around 770 nm, similar to others' results [15]. The PL intensity was markedly decreased when F_{16}CuPc was employed, which could be caused by the significantly enhanced charge carrier extraction arising from the added F_{16}CuPc layer. At the same time, when PEDOT:PSS and

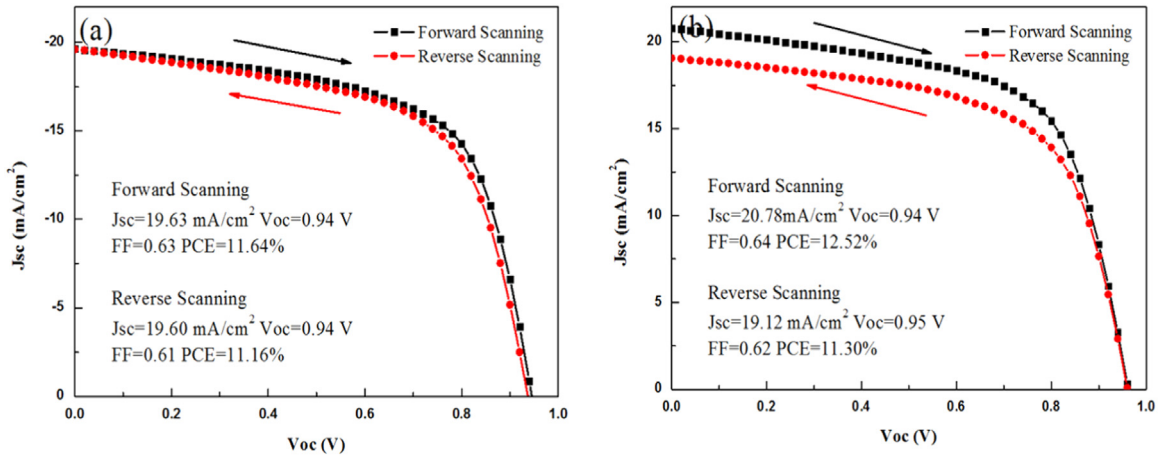

Fig. 6. J–V curves measured at forward and reverse scanning model for the devices with (a) F_{16}CuPc and (b) C_{60} as ETLs.

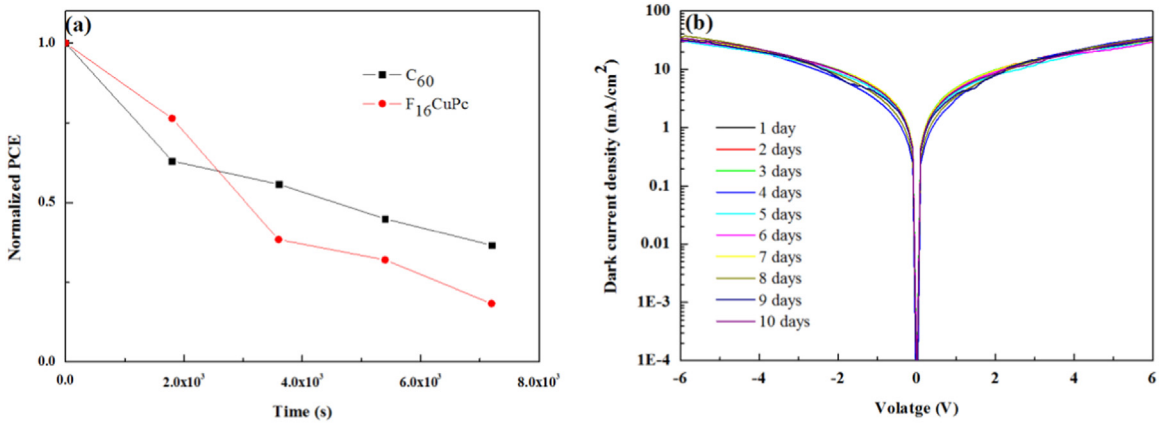

Fig. 8. (a) Normalized PCE comparison of the PSCs with F_{16}CuPc and C_{60} as ETLs during the first 120 min operation under 100 mW/cm^2 continuous illumination. (b) Current density changes as a function of the ageing time for the F_{16}CuPc-based electron-only devices stored under ambient condition.

F_{16}CuPc were both employed, PL from $CH_3NH_3PbI_3$ was nearly completely quenched. Clearly, free charges (or excitons) generated in $CH_3NH_3PbI_3$ upon illumination are extracted (or dissociated) by bottom layer of PEDOT: PSS and the top layer of F_{16}CuPc. These observations indicate that F_{16}CuPc is indeed a good ETL for PSCs and could play a role as an ETL in much the same way as fullerenes do.

Metallophthalocyanines (MPcs) are insoluble in water and many organic solvents and are relative stable materials. Particularly, for F_{16}CuPc, its 1.6 eV lower LUMO level than its unsubstituted counterpart makes it less susceptible to oxidation [38]. In addition, since all the F_{16}CuPcs adopt the edge-on conformations in their thin films, the fluorine atoms are in contact with air and could help to block moisture from penetrating through the films [39]. Thanks to the stability of F_{16}CuPc, a series of air-stable optoelectronic devices had been designed, which offer signs of hope to fabricate PSCs with better stability using F_{16}CuPc [22]. To explore this, the stability of PSCs with F_{16}CuPc as ETLs were estimated with the operation life. The operation life of C_{60}-based device was also studied for comparison. Fig. 8a shows the PCE values as a function of operation time under 100 mW/cm^2 continuous illumination for the devices with F_{16}CuPc and C_{60} as ETLs respectively. Unfortunately, improvement of device operation stability did not observed by replacing C_{60} with F_{16}CuPc as ETLs and both devices degraded very quickly under a continuous illumination. We deduce that operation stability of the PSCs here is mainly restricted by some other reasons such as the acidity of PEDOT: PSS, the corrosion of Al electrode by the perovskite, or the unstable of the perovskite itself, and hence change of ETLs does not influence device stability significantly. To verify the possibility of the improvement of PSCs with F_{16}CuPc as ETL, electron-only devices with the structure of ITO/BPhen (10 nm)/F_{16}CuPc/BPhen (10 nm)/Al (100 nm) were designed. Fig. 8b shows the current density changes as a function of the ageing time for the electron-only devices stored under ambient condition. After storing in 10 days, current density of the F_{16}CuPc-based electron-only devices changes very little indicating electron transport property of F_{16}CuPc changes slightly. Although we failed to improve the stability of PSC devices, the good environmental stability of the F_{16}CuPc demonstrated here strongly predicts the possibility of employing F_{16}CuPc for efficient and stable PSC designing in the future.

4. Conclusions

In summary, we have successfully demonstrated organic – inorganic hybrid PSCs with F_{16}CuPc as electron conductor and perovskite of $CH_3NH_3PbI_3$ as the light harvester for the first time. The best F_{16}CuPc-based photovoltaic devices displayed a considerably high PCE of 12.62% with a Jsc, Voc, and FF of 19.97 mA/cm^2, 0.93 V and 0.68, respectively. Such performance is among the highest performance for the PSCs with bilayer planar heterojunction devices in an inverted layout without employing a fullerene as ETL. Our results show that free charges are expected to be generated spontaneously following light absorption, as opposed to a large population of bound excitons. The development of the small molecule of F_{16}CuPc as a replacement to unstable fullerene provides a novel choice of the electron conductor in PSCs and may also have its application in some other photoelectric devices such as perovskite light-emitting diodes and perovskites photodetectors.

Acknowledgments

This work was supported by the National Natural Science Foundation of China Grants (61376062, 61376022, 61575192 and 61504145) and the Science and Technology Development Plan of Jilin Province (20140101094JC).

References

[1] N.J. Jeon, J.H. Noh, W.S. Yang, Y.C. Kim, S. Ryu, J. Seo, S.I. Seok, Compositional engineering of perovskite materials for high-performance solar cells, Nature 517 (2015) 476–480.
[2] S.D. Stranks, G.E. Eperon, G. Grancini, C. Menelaou, M.J. Alcocer, T. Leijtens, L. M. Herz, A. Petrozza, H.J. Snaith, Electron-hole diffusion lengths exceeding 1 μm in an organometal trihalide perovskite absorber, Science 342 (2013) 341–344.
[3] H. Zhou, Q. Chen, G. Li, S. Luo, T.B. Song, H.S. Duan, Z. Hong, J. You, Y. Liu, Y. Yang, Photovoltaics. Interface engineering of highly efficient perovskite solar cells, Science 345 (2014) 542–546.
[4] H.S. Kim, C.R. Lee, J.H. Im, K.B. Lee, T. Moehl, A. Marchioro, S.J. Moon, R. Humphry-Baker, J.H. Yum, J.E. Moser, M. Gratzel, N.G. Park, Lead iodide perovskite sensitized all-solid-state submicron thin film mesoscopic solar cell with efficiency exceeding 9%, Sci. Rep. 2 (2012) 591.
[5] J. Shi, Y. Luo, H. Wei, J. Luo, J. Dong, S. Lv, J. Xiao, Y. Xu, L. Zhu, X. Xu, H. Wu, D. Li, Q. Meng, Modified two-step deposition method for high-efficiency TiO2/CH3NH3PbI3 heterojunction solar cells, ACS Appl. Mater. Interfaces 6 (2014) 9711–9718.
[6] H.S. Jung, N.G. Park, Perovskite solar cells: from materials to devices, Small 11 (2015) 10–25.
[7] E. Edri, S. Kirmayer, A. Henning, S. Mukhopadhyay, K. Gartsman, Y. Rosenwaks, G. Hodes, D. Cahen, Why lead methylammonium tri-iodide perovskite-based solar cells require a mesoporous electron transporting scaffold (but not necessarily a hole conductor), Nano Lett. 14 (2014) 1000–1004.
[8] Z. Liu, T. Shi, Z. Tang, B. Sun, G. Liao, Using a low-temperature carbon electrode for preparing hole-conductor-free perovskite heterojunction solar cells under high relative humidity, Nanoscale 8 (2016) 7017–7023.

[9] X. Zhou, P. Gao, S. Sun, D. Bao, Y. Wang, X. Li, T. Wu, Y. Chen, P. Yang, Amorphous, crystalline and crystalline/amorphous selenium nanowires and their different (De)lithiation mechanisms, Chem. Mater. 27 (2015) 6730–6736.
[10] Z. Wei, H. Chen, K. Yan, S. Yang, Inkjet printing and instant chemical transformation of a CH3NH3PbI3/nanocarbon electrode and interface for planar perovskite solar cells, Angew. Chem Int Ed. Engl. 53 (2014) 13239–13243.
[11] H. Chen, Z. Wei, X. Zheng, S. Yang, A scalable electrodeposition route to the low-cost, versatile and controllable fabrication of perovskite solar cells, Nano Energy 15 (2015) 216–226.
[12] J.Y. Jeng, Y.F. Chiang, M.H. Lee, S.R. Peng, T.F. Guo, P. Chen, T.C. Wen, CH3NH3PbI3 perovskite/fullerene planar-heterojunction hybrid solar cells, Adv. Mater. 25 (2013) 3727–3732.
[13] C. Kuang, G. Tang, T. Jiu, H. Yang, H. Liu, B. Li, W. Luo, X. Li, W. Zhang, F. Lu, J. Fang, Y. Li, Highly efficient electron transport obtained by doping PCBM with graphdiyne in planar-heterojunction perovskite solar cells, Nano Lett. 15 (2015) 2756–2762.
[14] P.W. Liang, C.Y. Liao, C.C. Chueh, F. Zuo, S.T. Williams, X.K. Xin, J. Lin, A.K. Jen, Additive enhanced crystallization of solution-processed perovskite for highly efficient planar-heterojunction solar cells, Adv. Mater. 26 (2014) 3748–3754.
[15] S. Sun, T. Salim, N. Mathews, M. Duchamp, C. Boothroyd, G. Xing, T.C. Sum, Y. M. Lam, The origin of high efficiency in low-temperature solution-processable bilayer organometal halide hybrid solar cells, Energy Environ. Sci. 7 (2014) 399–407.
[16] H. Gommans, T. Aernouts, B. Verreet, P. Heremans, As Medina, C.G. Claessens, T. Torres, Perfluorinated subphthalocyanine as a new acceptor material in a small-molecule bilayer organic solar cell, Adv. Funct. Mater. 19 (2009) 3435–3439.
[17] O.K. Kwon, J.H. Park, D.W. Kim, S.K. Park, S.Y. Park, An all-small-molecule organic solar cell with high efficiency nonfullerene acceptor, Adv. Mater. 27 (2015) 1951–1956.
[18] A. Hamed, Y.Y. Sun, Y.K. Tao, R.L. Meng, P.H. Hor, Effects of oxygen and illumination on the insitu conductivity of C60 thin films, Phys. Rev. B 47 (1993) 10873–10880.
[19] T. Zhuang, Z. Su, Y. Liu, B. Chu, W. Li, J. Wang, F. Jin, X. Yan, B. Zhao, F. Zhang, D. Fan, Improvement of both efficiency and working lifetime in organic photovoltaic devices by using bathophenanthroline/tin(IV) phthalocyanine dichloride as bilayer exciton blocking layers, Appl. Phys. Lett. 100 (2012) 243902.
[20] M. Hermenau, M. Riede, K. Leo, S.A. Gevorgyan, F.C. Krebs, K. Norrman, Water and oxygen induced degradation of small molecule organic solar cells, Sol. Energy Mater. Sol. Cells 95 (2011) 1268–1277.
[21] G.E. Morse, T.P. Bender, Boron subphthalocyanines as organic electronic materials, ACS Appl. Mater. Interfaces 4 (2012) 5055–5068.
[22] R. Ye, M. Baba, Y. Oishi, K. Mori, K. Suzuki, Air-stable ambipolar organic thin-film transistors based on an organic homostructure, Appl. Phys. Lett. 86 (2005) 253505.
[23] J. Burschka, N. Pellet, S.J. Moon, R. Humphry-Baker, P. Gao, M.K. Nazeeruddin, M. Gratzel, Sequential deposition as a route to high-performance perovskite-sensitized solar cells, Nature 499 (2013) 316–319.
[24] H. Chen, Z. Wei, H. He, X. Zheng, K.S. Wong, S. Yang, Solvent engineering boosts the efficiency of paintable carbon-based perovskite solar cells to beyond 14%, Adv. Energy Mater. (2016) (n/a-n/a).
[25] F. Hou, Z. Su, F. Jin, X. Yan, L. Wang, H. Zhao, J. Zhu, B. Chu, W. Li, Efficient and stable planar heterojunction perovskite solar cells with an MoO3/PEDOT: PSS hole transporting layer, Nanoscale 7 (2015) 9427–9432.
[26] S.-S. Kim, S.-Y. Choi, C.-G. Park, H.-W. Jin, Transparent conductive ITO thin films through the sol-gel process using metal salts, Thin Solid Films 347 (1999) 155–160.
[27] L. Etgar, P. Gao, Z. Xue, Q. Peng, A.K. Chandiran, B. Liu, M.K. Nazeeruddin, M. Gratzel, Mesoscopic CH3NH3PbI3/TiO2 heterojunction solar cells, J. Am. Chem. Soc. 134 (2012) 17396–17399.
[28] G.R. Perumallapelli, S.R. Vasa, J. Jang, Improved morphology and enhanced stability via solvent engineering for planar heterojunction perovskite solar cells, Org. Electron. 31 (2016) 142–148.
[29] Q. Chen, H. Zhou, Z. Hong, S. Luo, H.S. Duan, H.H. Wang, Y. Liu, G. Li, Y. Yang, Planar heterojunction perovskite solar cells via vapor-assisted solution process, J. Am. Chem. Soc. 136 (2014) 622–625.
[30] G. Xing, N. Mathews, S. Sun, S.S. Lim, Y.M. Lam, M. Gratzel, S. Mhaisalkar, T. C. Sum, Long-range balanced electron- and hole-transport lengths in organic-inorganic CH3NH3PbI3, Science 342 (2013) 344–347.
[30] L. Zheng, Y. Ma, S. Chu, S. Wang, B. Qu, L. Xiao, Z. Chen, Q. Gong, Z. Wu, X. Hou, Improved light absorption and charge transport for perovskite solar cells with rough interfaces by sequential deposition, Nanoscale 6 (2014) 8171–8176.
[32] X. Jiang, J. Dai, H. Wang, Y. Geng, D. Yan, Organic photovoltaic cells using hexadecafluorophthalocyaninatocopper (F16CuPc) as electron acceptor material, Chem. Phys. Lett. 446 (2007) 329–332.
[33] J.L. Yang, P. Sullivan, S. Schumann, I. Hancox, T.S. Jones, Organic photovoltaic cells based on unconventional electron donor fullerene and electron acceptor copper hexadecafluorophthalocyanine, Appl. Phys. Lett. 100 (2012) 023307.
[34] M.C. Scharber, D. Mühlbacher, M. Koppe, P. Denk, C. Waldauf, A.J. Heeger, C. J. Brabec, Design rules for donors in bulk-heterojunction solar cells—towards 10% energy-conversion efficiency, Adv. Mater. 18 (2006) 789–794.
[35] J. Even, L. Pedesseau, C. Katan, Analysis of multivalley and multibandgap absorption and enhancement of free carriers related to exciton screening in hybrid perovskites, J. Phys. Chem. C 118 (2014) 11566–11572.
[36] S.D. Stranks, V.M. Burlakov, T. Leijtens, J.M. Ball, A. Goriely, H.J. Snaith, Recombination kinetics in organic-inorganic perovskites: excitons, free charge, and subgap states, Phys. Rev. Appl. 2 (2014).
[37] C. Sheng, C. Zhang, Y. Zhai, K. Mielczarek, W. Wang, W. Ma, A. Zakhidov, Z. V. Vardeny, Exciton versus free carrier photogeneration in organometal trihalide perovskites probed by broadband ultrafast polarization memory dynamics, Phys. Rev. Lett. 114 (2015) 116601.
[38] E. Karmann, J.P. Meyer, D. Schlettwein, N.I. Jaeger, M. Anderson, A. Schmidt, N. R. Armstrong, Photoelectrochemical effects and (Photo)conductivity of "N-Type" phthalocyanines, Mol. Cryst. Liq. Cryst. Sci. Technol. Sect. A. Mol. Cryst. Liq. Cryst. 283 (1996) 283–291.
[39] Z. Bao, A.J. Lovinger, J. Brown, New air-stable n-channel organic thin film transistors, J. Am. Chem. Soc. 120 (1998) 207–208.